Journal Title
XX(X):1–10

DOI: 10.1177/ToBeAssigned
www.sagepub.com/
SAGE

High voltage synthetic inductor for vibration damping in resonant piezoelectric shunt

Kevin Dekemele[1], Patrick Van Torre[2] and Mia Loccufier[1]

Abstract

Resonant piezoelectric shunts are a well established way to reduce vibrations of mechanical systems suffering from resonant condition. The vibration energy is transferred to the electrical domain through the bonded piezoelectrical material (PEM) where it is dissipated in the shunt. Typically, electrical and mechanical resonance frequencies are several orders apart. As such, finding a suitable high inductance component for the resonant shunt is not feasible. Therefore, these high inductance values are mimicked through synthetic impedances, consisting of operational amplifiers (OpAmps) and passive components. A downside of these synthetic impedances is that standard OpAmps can only handle op to 30V peak-to-peak and the state of the art amplifiers up to 100Vpp. However, as mechanical structures tend to become lighter and more flexible, the order induced voltages over de PEM's electrodes voltages increases above these limitations. In this research, a high voltage synthetic inductor is proposed and built by combining the bridge amplifier configuration and the output voltage boost configuration around a single OpAmp gyrator circuit, effectively quadrupling the range of the synthetic inductor to 400Vpp. The impedance of the circuit over a frequency range is numerically and experimentally investigated. The synthetic inductor is then connected to a PEM bonded to a cantilever beam. Numerical and experimental investigation confirm the high-voltage operation of the implemented circuit and its suitability as a vibration damping circuit.

Keywords

Structural Vibrations, Piezoelectric Shunt, Synthetic Impedance

1 Introduction

To mitigate vibration levels in mechanical structures, typically tuned mass damper (TMD) Den Hartog (1934) are locally attached to this structure. This is a passive mechanical oscillator sensitive to the resonance frequency of the mechanical structure. The TMD not only ensures transfer of energy from the structure to the TMD, it also dissipates it. As a result the vibration levels in the structure are significantly reduced. While a TMD is a purely mechanical device, it is also possible to transfer the mechanical vibration energy of the structure into the electrical domain. This is done by bonding piezoelectric material (PEM) to the structure. As the vibrating structure strains the PEM, a voltage is induced over the PEM's electrodes. Shunting these electrodes with a resonant electrical circuit reduces the vibrations in the structure in the same way as TMD Hagood and von Flotow (1991). In their respective engineering fields, electrical and mechanical resonance frequencies are typically several orders apart. Therefore, enormous inductance values are required in the shunt, at-least compared to off-the-shelf inductors, to closely match the resonance frequency of mechanical structure and in the electrical shunt. Although wirewound inductor coils with high inductance values have been designed for use in resonant shunts Lossouarn et al. (2017), it involves a highly specialized process and are not readily available. Furthermore, magnetic saturation in the inductor's core limits their voltage range. Therefore, large inductances are often realized in a synthetic impedance circuit i.e., an active electronic circuit which mimics the impedance of an inductor. These circuits consists of operational amplifiers (OpAmps), passive resistors and capacitors. No magnetic cores are involved. An additional advantage of these synthetic impedances, is that the inductance value can easily be adjusted with variable resistor. A downside of these synthetic impedance is that OpAmps have limited voltage ranges. Typically, ordinary OpAmps saturate for voltage levels above 30 Vpp. Mechanical design trend towards more slender and lighter structures, creating more flexible structures with increased vibration levels. These high levels might induce voltage well over 100 V. Therefore, mostly submillimeter or even submicrometer vibration levels are used in experiments with synthetic impedance Thomas et al. (2011); Neubauer et al. (2006); dell'Isola et al. (2004).

A state-of-the-art commercially available high voltage OpAmp is the OPA445 (90V peak-to-peak) Texas Instruments (2008), often used in literature when designing a synthetic inductor dell'Isola et al. (2004); Berardengo et al. (2018), or more advanced, a negative capacitance Neubauer et al. (2006) and more recently digital impedances Nečásek et al. (2016). The OPA454 (100Vpp) is another high-voltage, more advanced, OpAmp Texas Instruments (2016).

[1]Department of Electromechanical, Systems and Metal Engineering, Ghent University [2]Department of Information Technology, Ghent University

Corresponding author:
Kevin Dekemele, DySC research group, Department of Electromechanical, Systems and Metal Engineering, Ghent University, Tech Lane Ghent Science Park Campus A, 125 9052, Ghent, Belgium
Email: kevin.dekemele@ugent.be

It has an exposed metal pad for cooling the chip. Because it only ships in the SMD-package, it cannot be used in a breadboard and is more difficult to solder. Therefore, its only rarely used in synthetic impedance circuits Wang et al. (2017). A first high-voltage shunt was designed in Heuss et al. (2016), were it was claimed the shunt could handle 350 Vpp. However, the design of this circuit was not disclosed. At first sight another solution seems to exist in the form of a single amplifier, directly supplied at a very high-voltage power supply. According to its data sheet APEX Microtechnology (2012), the APEX PA78, for example, can operate up to a power-supply level of 350 V but is an expensive component, provided by only a limited number of suppliers. Moreover, according to its data sheet, the PA78 is designed as a high speed pulse amplifier and internally quite different from a normal OpAmp. Signal-dependent output impedance as well as stability issues are expected make the design of a gyrator circuit quite challenging. Additionally the amplifier's differential input voltage is limited to 16 V, requiring extra voltage-limiting protection circuits. The OPA454 high-voltage OpAmp, in contrast, does not have these disadvantages and, importantly, is specified as unity-gain stable.

To boost the range of OpAmps, there are several known techniques. The most straightforward one is the *bridge amplifier configuration*. Here, two similar amplifiers are driven anti-phase. The load is connected between the two amplifier outputs, effectively doubling the output voltage range. Another, less commonly implemented, strategy is the *output voltage boost configuration*. In this configuration, the positive and negative supply of the amplifier is supplied by two auxiliary supply boost amplifiers. The supply voltages of the main amplifier is adjusted dynamically to accommodate changing voltage levels. By carefully selecting proper boost amplifier supplies and gain factors, the effective output voltage range can be doubled. By combining both techniques, the voltage range can be increased by fourfold.

The aim of this research is to design a synthetic inductor capable of handling high voltage levels. This way, vibration mitigation with piezoelectric shunts can be applied beyond small amplitude lab setups, to applications with high vibration levels. Furthermore, this must to done for a low component cost. Therefore, a 400V boosted synthetic inductor with the OPA454 amplifier is designed and built to serve as a resonant shunt. To reduce components, this circuit is based around a single OpAmp Gyrator circuit National Semiconductor (1994), which approximates a synthetic inductor. In the current paper, this circuit will be put in bridge amplifier configuration and voltage boost configuration. Thus, a total of 6 OPA 454 OpAmps are needed for the high-voltage operation. The most frequently employed synthetic inductor is the Antoniou circuit in Vatavu et al. (2019). Although this setup allows lower internal resistance than the single-OpAmp Gyrator/ Our proposed technique for quadrupling the output voltage for the Antoniou circuit would double the number of required OpAmps from 6 to 12, as each OpAmp would need its separate supply boost circuit, increasing component cost and complexity. However, the gyrator circuit has less ideal properties regarding resistance. This research also discussed under which conditions the gyrator is suitable as a resonant shunt. The here built 400V synthetic inductor circuit is used experimentally as a resonant shunt to reduce the vibrations in flexible cantilever beam. The measured deflection of the beam under resonance with and without resonant shunt confirms the expected mitigation.

The proposed technique for boosting the operational voltage range can be extended to a number of other circuits, such as negative or nonlinear capacitors. The paper further describes the single-OpAmp gyrator, boost and bridge configurations, power supply and impedance measurements in Section 2. The electromechanical system model and tuning of the gyrator are outlined in Section 3, including simulations and a practical experiment. Finally, the conclusions are presented in Section 4

2 High voltage synthetic inductor

2.1 Single OpAmp gyrator

At the heart of the high-voltage synthetic inductor is a single OpAmp gyrator, with the circuit scheme given in Figure 1. This circuit has an equivalent impedance of a passive RL-circuit. To realize this circuit, the OPA454 OpAmp will be used. This OpAmp has the highest voltage range for commercially available OpAmps. The OPA454 is specified at 100V (or +50V and -50V) supply voltage, with an absolute maximum rating of 120V. OpAmps can only output signals within their supply voltage range.

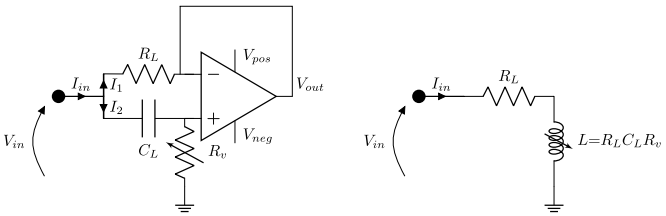

Figure 1. High-voltage gyrator with OPA454 OpAmp

The equivalent impedance is given by Ohm's law as

$$Z_{in} = \frac{V_{in}}{I_{in}} = \frac{V_{in}}{I_1 + I_2} \tag{1}$$

The OpAmp is configured as a voltage buffer. Assuming an ideal OpAmp, then $V_+ = V_-$ because of the feedback. The output voltage of the OpAmp is then:

$$V_{out} = V_{in} \cdot \frac{R_v}{R_v + \frac{1}{j\omega C_L}} = V_{in} \cdot \frac{j\omega R_v C_L}{1 + j\omega R_v C_L} \tag{2}$$

Under the ideal OpAmp assumption, no current flows in the $+$ and $-$ terminals of the OpAmp. So, the currents I_1 and I_2 are:

$$I_1 = \frac{V_{in} - V_{out}}{R_L} \quad I_2 = \frac{V_{in}}{R_v + \frac{1}{j\omega C_L}} \tag{3}$$

Combining equations (1), (2) and (3):

$$Z_{in} = \frac{R_L}{1 + \frac{R_L - R_v}{R_v + \frac{1}{j\omega C_L}}} = R_L \frac{j\omega C_L R_v + 1}{j\omega C_L R_L + 1} \tag{4}$$

or by splitting into real and imaginary parts:

$$Z_{in} = R_L \frac{1+(\omega C_L)^2 R_v R_L}{(\omega C_L R_L)^2+1} + jR_L \frac{\omega C_L (R_v - R_L)}{(\omega C_L R_L)^2+1} \quad (5)$$

If the components are chosen such that $\omega C_L R_L \ll 1$ and $R_L \ll R_v$, the resulting impedance is approximated as

$$Z_{in} \approx R_L + j\omega R_v C_L R_L \quad (6)$$

The impedance of the gyrator is approximately equivalent to an inductor with a value of $C_L R_v R_L$ H, in series with a small resistor R_L. The exact impedance given in equation (5) has a complex depence of ω, such that this approximation only holds within a range of ω.

In literature, the most popular synthetic inductor is the 2-OpAmp Antoniou circuit dell'Isola et al. (2004); Berardengo et al. (2018); Thomas et al. (2011). That circuit does not have the equivalent series resistor. The presence of an equivalent resistance of the gyrator does not compromise the performance of the vibration damping as intended as resonant shunts do require a significant series resistance Thomas et al. (2011) for broadband performance.

2.2 Effect of gyrator tuning on resistance

The mechanical system where the PEM is bonded to, has a mechanical resonance frequency ω_n. In the tuning procedure explained later on in Section 3.1, the gyrator is tuned such that the electrical resonance frequency, caused by the inductance of the gyrator and the capacitance of the PEM, approximates the mechanical one:

$$\frac{1}{LC_p} \approx \omega_n^2 \quad (7)$$

with C_p the capacitance of the shunted PEM. The variable resistor R_v in the gyrator circuit should thus be tuned to $R_v = \frac{L}{CR_l}$. The real part of the impedance in equation (5) then is:

$$R_{gyr}(\omega) = \frac{R_L}{C_p} \frac{C_p + C_L}{(\omega C R_L)^2 + 1} \quad (8)$$

Which is maximum for $\omega_n = 0$, $R_v = \frac{R_L}{C_p}(C_p + C_L)$. This resistance is thus greater than the approximation in (1). Wether or not this resistance is too high for optimal tuning, will be elaborated further in Section 3.2.

2.3 Power supply boost configuration

A first way to extend the voltage range of an amplifier is by dynamically adapting the OpAmp's supply voltages depending on the desired output voltage. To achieve this, the power supplies V_{pos} and V_{neg} of the gyrator circuit in Figure 1, are supplied by two auxiliary OPA454 OpAmps, one adapting the V_{pos} and the other adapting the V_{neg} . The now 3-OpAmp circuit scheme is given in Figure 2.

The supply boost auxiliary OpAmps are configured as an equal-resistor buffered voltage divider between the gyrator's output voltage and the positive or negative power supply voltage (here +100 and -100 V). The supplied voltages of the gyrator are:

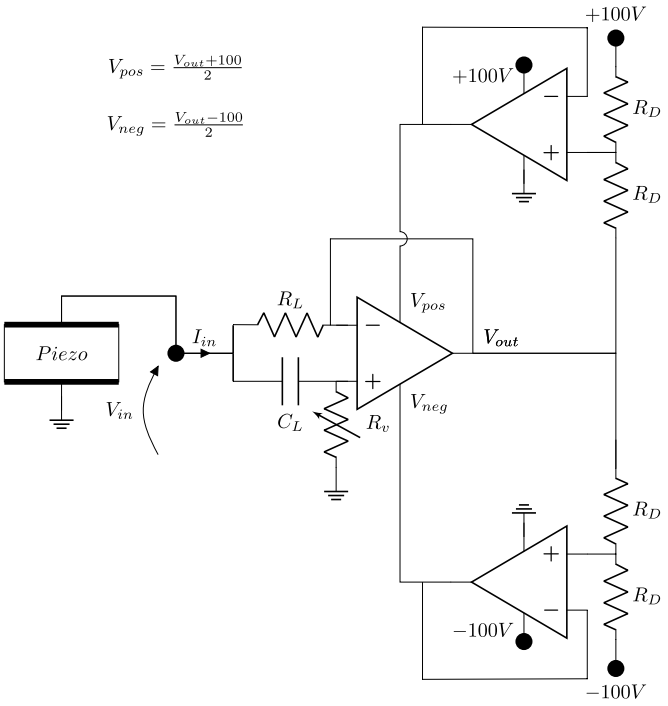

Figure 2. The gyrator with power supply boost.

$$\begin{aligned} V_{pos} &= \frac{V_{out} + 100V}{2} \\ V_{neg} &= \frac{V_{out} - 100V}{2} \end{aligned} \quad (9)$$

The gyrator's output voltage range is now extended to $200V_{pp}$ as the power supply voltages track the output voltage when referring to ground level, whereas the total supply voltage accross the central OpAmp always remains equal to

$$V_{supply} = V_{pos} - V_{neg} = 100V \quad (10)$$

well within the absolute maximum rating of 120V specified for the OPA454 Texas Instruments (2016).

The operation is illustrated by means of $200V\,pp$ sine wave in Figure 4. In this graph the power supply boosted gyrator is driven to its full output voltage range on a ±100V symmetric power supply.

2.4 Bridge configuration

To extend to voltage range even further, the Bridge Tied Load (BTL) configuration will be applied. In the field of amplifier design, it is often used to deliver an output amplitude which is double the voltage range of an single amplifier. This is done by driving two amplifiers anti-phase, and then connecting them both to the load. On Figure 3, the left and right boosted gyrators are indeed driven antiphase, with the piezo element PE functioning as a source in between the two outputs, sourcing current in one terminal and sinking the same current from the other terminal. Basically two synthetic inductors with voltage boost configuration are employed in series, effectively quadrupling the output voltage range of a single gyrator to $400V_{pp}$.

Because the piezoelectric transducer is connected between the two gyrators, these gyrators appear in series with respect to the piezoelectric transducer. The total synthetic impedance

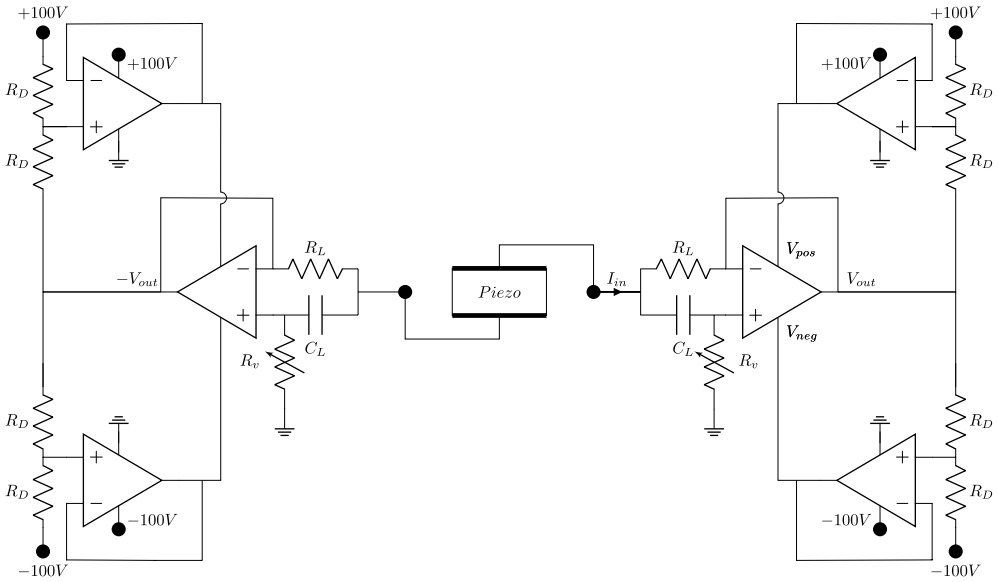

Figure 3. Extending the voltage range of a synthetic inductor with Power Supply Boost and Bridge configuration. Voltages determined based on antisymmetric excitation by the central piezo element PE.

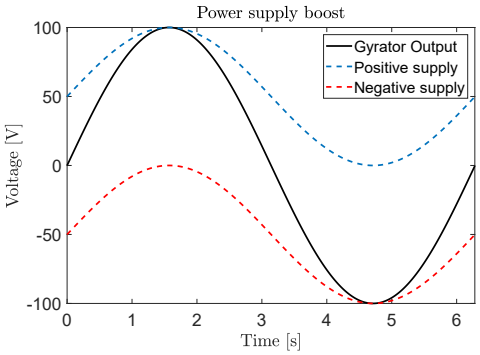

Figure 4. Power supply boost operation

over the piezo's electrodes is thus a sum of the impedance of the two voltage-boosted gyrators. Choosing similar component values in both gyrator circuits, the approximate impedance approximately equals

$$Z \approx 2j\omega C_L \cdot R_v \cdot R_L + 2R_L \tag{11}$$

For example, off-the-shelf component values are $C_L = 1\mu F$, $R_v = 1M\Omega$ and $R_L = 100\Omega$, achieving an inductance of 200H in series with a 200Ω resistor. In the realization of the circuit, R_v is adjusted by a $1M\Omega$ variable resistor, allowing to change the inductance from 0 to 200H. Figures 9a and 9b show the experimentally constructed, 400V gyrator circuit.

2.5 Power interface

According to the circuit diagram presented in Figure 3, a 100V DC and -100V DC power source needed to power the whole circuit. These voltages are not readily available. To increase the portability of the designed circuit, modular of-the-shelf DC-DC convertor units were included to transform a standard 12V DC supply to the internally needed +100V and -100V. The advantage is that no dangerous high-voltage DC supplies are needed externally, and the 12V DC supply does not draw much current and is can hence be provided with a common DC adapter.

2.6 Experimental impedance measurements

The impedance of the gyrator has been measured employing a Rohde & Schwartz RTM3000 oscilloscope in Bode Plot mode, with the gyrator placed in an RL network with a 10 $k\Omega$ resistor. A signal is automatically swept over a frequency range of 10 to 200 Hz and data exported to MATLAB. As the measurement suffers from noise and 500 measurement point are available a moving average over 10 measurements is employed on the complex samples to suppress the measurement noise. For the components $C_L = 1\mu F$, $R_L = 100\Omega$ and variable resistor $R_v = 1M\Omega$, the experimental and theoretical impedance from equation (5) are shown in Figures 5a and 5b. The variable resistor is put on 3 settings, low resistance, quarter setting and full setting. The inductance L is fairly constant throughout the measured frequency range, however the resistance is not. The resistance increases almost 100-fold over the whole frequency range. For a given frequency, the resistance is higher for higher inductances. The effect of this highly variable resistance on tuning is quantitatively discussed in Section 3.2, where a range of frequencies is found where the gyrator can be tuned as a resonant shunt.

3 Electromechanical System

3.1 Theoretical model and tuning

To experimentally test the high voltage gyrator, it will be used to damp vibrations of a cantilever beam. The beam will be bonded with 2 PE patches near its fixed end, as shown on Figure 6. One PE patch serves as an actuator to induce vibrations in the beam, while the other will be shunted with the gyrator.

The dynamic deflection along x, $u(x)$ is expressed in a spatial mode shape and a modal time coordinate $u(x,t) = \varphi(x)r(t)$, the dynamical equation of the full system can be written as Leo (2007)

$$\begin{cases} m\ddot{r} + c\dot{r} + k^E r - \theta_2 V_2 = \theta_1 V_1 + \varphi(L_f)F \\ C_{p,2}V_2 + \theta_2 r = q \end{cases} \tag{12}$$

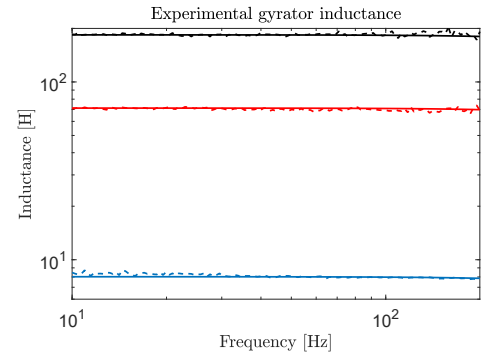

(a)

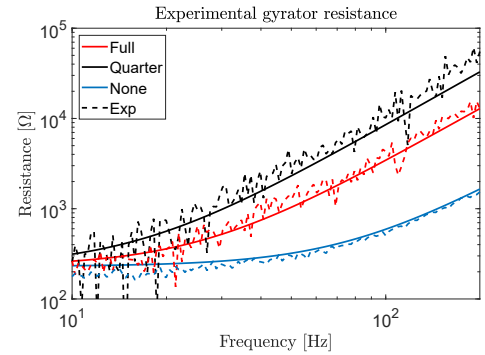

(b)

Figure 5. Theoretical (full) and measured impedance (dashed), inductance (a) and resistance (b) for 3 settings of variable resistor

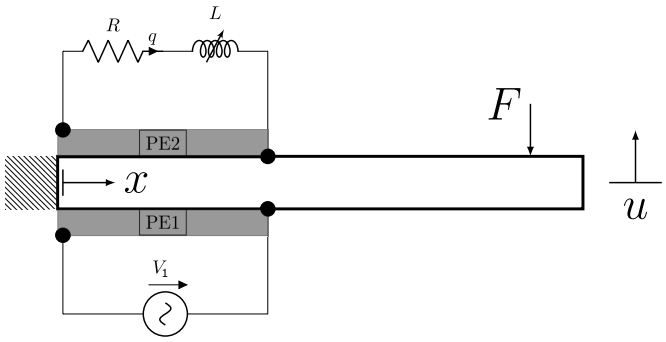

Figure 6. The considered dynamical system, a cantilever beam with PE1 used as an actuator and PE2 shunted with a RL shunt

with m the modal mass, c the modal damping, k^E the closed circuit modal stiffness, θ_1 the modal coupling coefficient of the actuating piezo, θ_2 the modal coupling coefficient of the shunted piezo and $C_{p,2}$ the capacitance of the shunted piezo. In what follows, the forcing term will be omitted as in the experiment only V_1 will be used to excite the beam. Note that the model in equation (12) not only describes a cantilever beam but also any 1-dimensional vibrating mechanical system bonded with piezoelectric patches.

For open circuit, closed circuit, ideal resonant shunt and gyrator, the dynamics are written in state space form:

$$\begin{aligned}\dot{\mathbf{x}} &= \mathbf{A}\mathbf{x} + \mathbf{B}\mathbf{u} \\ \mathbf{y} &= \mathbf{C}\mathbf{x}\end{aligned} \tag{13}$$

The actuating voltage $\mathbf{u} = V_1$ is the input and the tip displacement of the beam and voltage of the damping shunt are the output, $\mathbf{y} = \begin{bmatrix} u(L_b) \\ V_2 \end{bmatrix}$. The frequency responses are then calculated from the state space with $\mathbf{G}(j\omega) = \begin{bmatrix} G_{V_1 u(L_b)}(j\omega) \\ G_{V_1 V_2}(j\omega) \end{bmatrix} = \mathbf{C}(-j\omega - \mathbf{A})^{-1}\mathbf{B}$

3.1.1 Closed circuit When the damping piezo's electrodes are short-circuited, $V_2 = 0$ in equation (12), the state space is:

$$\begin{bmatrix} \dot{r} \\ \ddot{r} \end{bmatrix} = \begin{bmatrix} 0 & 1 \\ -\frac{k^E}{m} & -\frac{c}{m} \end{bmatrix} \begin{bmatrix} r \\ \dot{r} \end{bmatrix} + \begin{bmatrix} 0 \\ \frac{\theta_1}{m} \end{bmatrix} V_1 \tag{14}$$

The output of the state space is:

$$\begin{bmatrix} u(L_b) \end{bmatrix} = \begin{bmatrix} \varphi(L_b) & 0 \end{bmatrix} \begin{bmatrix} r \\ \dot{r} \end{bmatrix} \tag{15}$$

3.1.2 Open circuit When the damping piezo is left open circuit, $q = 0$ in equation (12), the state space is:

$$\begin{bmatrix} \dot{r} \\ \ddot{r} \end{bmatrix} = \begin{bmatrix} 0 & 1 \\ -\frac{k^D}{m} & -\frac{c}{m} \end{bmatrix} \begin{bmatrix} r \\ \dot{r} \end{bmatrix} + \begin{bmatrix} 0 \\ \frac{\theta_1}{m} \end{bmatrix} V_1 \tag{16}$$

with $k_D = k_E + \frac{\theta_2^2}{C_{p,2}}$, the open circuit modal stiffness. From the two stiffnesses, two resonance frequencies are defined

$$\omega_{OC}^2 = \frac{k^D}{m} \quad \omega_{SC}^2 = \frac{k^E}{m} \tag{17}$$

with ω_{OC}^2 the open circuit resonance frequency and ω_{SC}^2 the short circuit resonance frequency. The dimensionless effective modal electromechanical coupling k_{eff} is defined as:

$$k_{eff}^2 = \frac{\omega_{OC}^2 - \omega_{SC}^2}{\omega_{SC}^2} \tag{18}$$

which will be used for the tuning of the RL shunt, as this quantity is easily determined from experiments. The output of the state space is:

$$\begin{bmatrix} u(L_b) \\ V_2 \end{bmatrix} = \begin{bmatrix} \varphi(L_b) & 0 \\ -\frac{\theta_2}{C_{p,2}} & 0 \end{bmatrix} \begin{bmatrix} r \\ \dot{r} \end{bmatrix} \tag{19}$$

3.1.3 Resonant shunt If the damping piezo is shunted with an ideal resonant shunt, then $V_2 = -L\ddot{q} - R\dot{q}$. The describing dynamics now include electrical variables q and $\dot{q}$:

$$\begin{bmatrix} \dot{r} \\ \ddot{r} \\ \dot{q} \\ \ddot{q} \end{bmatrix} = \begin{bmatrix} 0 & 1 & 0 & 0 \\ -\frac{k^D}{m} & -\frac{c}{m} & \frac{\theta_2}{C_{p,2}m} & 0 \\ 0 & 0 & 0 & 1 \\ \frac{\theta_2}{C_{p,2}L} & 0 & -\frac{1}{LC_{p,2}} & -\frac{R}{L} \end{bmatrix} \begin{bmatrix} r \\ \dot{r} \\ q \\ \dot{q} \end{bmatrix} + \begin{bmatrix} 0 \\ \frac{\theta_1}{m} \\ 0 \\ 0 \end{bmatrix} V_1 \tag{20}$$

with the output:

$$\begin{bmatrix} u(L_b) \\ V_2 \end{bmatrix} = \begin{bmatrix} \varphi(L_b) & 0 & 0 & 0 \\ -\frac{\theta_2}{C_{p,2}} & 0 & \frac{1}{C_{p,2}} & 0 \end{bmatrix} \begin{bmatrix} r \\ \dot{r} \\ q \\ \dot{q} \end{bmatrix} \tag{21}$$

To tune the resonant shunt, the rules in Thomas et al. (2011) are applied. There, the resonant shunt was tuned with the equal-peak optimization. This method is based on tuning of a mechanical vibration absorber, Den Hartog (1934). The frequency response function of the amplitude shows 2 fixed points for any choice of R and L. In the equal-peak method,

the shunt is tuned such that the attenuation at these two fixed points is equal. This results in the following optimal R_{opt} and L_{opt} values:

$$\begin{aligned} \frac{1}{\sqrt{L_{opt}C_{p,2}}} &= \omega_{SC}\sqrt{1+k_{eff}^2} \\ \frac{R_{opt}}{2}\sqrt{\frac{C_{p,2}}{L_{opt}}} &= \sqrt{\frac{3}{8}}k_{eff} \end{aligned} \tag{22}$$

3.1.4 Gyrator The gyrator is not an ideal resonant shunt, as the full impedance in equation (5) and the experimental impedance measurements in Figure 5 revealed. To accomodate the complete impedance, the 4rth row of **A** in the state space in equation (20) is changed to:

$$\ddot{q} = \frac{1}{R_v C_L R_L}\left(\frac{(\theta_2\dot{r}-\dot{q})C_L R_L}{C_p} + \frac{\theta_2 r - q}{C_p} - (R_L + R_{add})\dot{q}\right) \tag{23}$$

with R_{add} an added resistance in series with the gyrator, in order to attain the optimal resistance of equation (22). It is calculated as $R_{add} = R_{opt} - R_{gyr}(\omega_{SC})$ with R_{gyr} given in equation (8).

3.2 Tuning of gyrator

The resonant shunt resistance and inductance are tuned according to the short-circuit resonance frequency of the electromechanical system, see equation (22). The inherent resistance of the gyrator, the real part of equation (5) should be lower than the optimal R_{opt}. The remaining resistance can simply be added. For a given ω_{SC}, k_{eff} and C_p:

$$\begin{aligned} R_{opt} > & R_{gyr} \Rightarrow \\ \frac{2\sqrt{\frac{3}{8}}k_{eff}}{\omega_{SC}\sqrt{1+k_{eff}^2}C_p} > & R_L\frac{1+(\omega C_L)^2 R_v R_L}{(\omega C_L R_L)^2+1} \end{aligned} \tag{24}$$

For an optimal inductance L_{opt}, the variable resistor of the gyrator R_v should be adjusted to:

$$R_v = \frac{L_{opt}}{C_L R_L} = \frac{1}{\omega_{SC}^2(1+k_{eff}^2)C_p C_L R_L} \tag{25}$$

Although this is the approximate inductance, (see imaginary part of equation (1)) the impedance measurements in Section 2.6 have shown that the inductance is constant over a large frequency range. The total resistance of the gyrator, when tuned to the optimal inductance is then:

$$R_{gyr} = \frac{R_L}{(1+k_{eff}^2)C_p}\frac{(1+k_{eff}^2)C_p + C_L}{(\omega_{SC}C_L R_L)^2+1} \tag{26}$$

which is maximum for $\omega_{SC} \to 0$ and decreases for increasing ω_{SC}.

The condition in equation (24) collected in terms of ω_{SC}:

$$\begin{aligned} &\sqrt{\frac{3}{8}}k_{eff}R_L^2 C_L^2 \omega_{SC}^2 - \left[\frac{R_L}{\sqrt{1+k_{eff}^2}}\left((1+k_{eff}^2)C_p + C_L\right)\right]\omega_{SC} \\ &+2\sqrt{\frac{3}{8}}k_{eff} > 0 \end{aligned} \tag{27}$$

Solving this inequality yields the range of frequencies where the gyrator can be optimally tuned. To analyze the inequality, it is simplified. The capacitance of PEM is typically in the order of nF, while capacitance in the gyrator circuits is in the order of μF. Therefore $(1+k_{eff}^2)C_p + C_L \approx C_L$ or

$$\begin{aligned} &2\sqrt{\frac{3}{8}}k_{eff}R_L^2 C_L^2 \omega_{SC}^2 - \left[\frac{1}{\sqrt{1+k_{eff}^2}}R_L C_L\right]\omega_{SC} \\ &+2\sqrt{\frac{3}{8}}k_{eff} > 0 \end{aligned} \tag{28}$$

This second order polynomial in ω_{SC} has the following discriminant:

$$\frac{R_L C_L}{1+k_{eff}^2}\left(1-6k_{eff}^2-6k_{eff}^4\right) \tag{29}$$

which is negative for $k_{eff} > 0.38$. Thus, the gyrator can always be optimally tuned provided the effective coupling is high enough. The solution of the inequality in equation(28) is :

$$\begin{aligned} \omega_{SC} < & \frac{1}{4\sqrt{1+k_{eff}^2}}\frac{1-\sqrt{1-6k_{eff}^2-6k_{eff}^4}}{\sqrt{\frac{3}{8}}k_{eff}R_L C_L} \\ \omega_{SC} > & \frac{1}{4\sqrt{1+k_{eff}^2}}\frac{1+\sqrt{1-6k_{eff}^2-6k_{eff}^4}}{\sqrt{\frac{3}{8}}k_{eff}R_L C_L} \end{aligned} \tag{30}$$

For the experimental setup, $k_{eff} = 0.14$ and $C_p = 100$ nF. For a gyrator with $R_L = 100\ \Omega$ and $C_L = 1\ \mu$F, the optimal resonance shunt can be tuned provided that $1610 > \omega_{SC} > 62103$. The optimal resistance and the gyrator resistance for optimal inductance are plotted in Figure 7 up to 500 Hz.

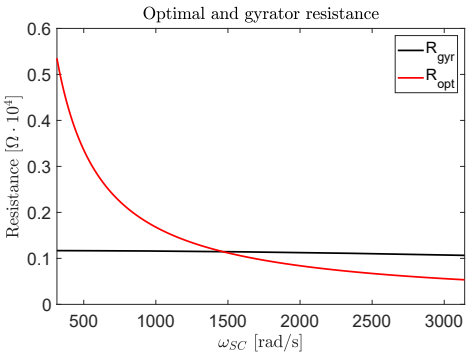

Figure 7. The optimal R compared to the inherent R of the gyrator, when tuned.

3.3 Numerical Simulation

To simulate the system in equation (12), is is assumed that the cantilever Euler-Bernouilli beam vibrates according its first mode, $\varphi(x) = \cosh(1.875\frac{x}{L_b}) - \cos(1.875\frac{x}{L_b}) - 0.734(\sinh(1.875\frac{x}{L_b}) - \sin(1.875\frac{x}{L_b})$, with beam and piezo parameters found on Table 1. The beam is aluminum and the piezoelectric patch is a DURA ACT patch by PI PI ceramics (2020), having the P225 piezoelectric material PI

ceramics (2008). The modal parameters of in equation (12) are obtained with energy-based modelling using Hamilton's principle Chopra and Sirohi (2013). The modal mass consists of contribution of the beam m_b and the piezoelectric patches, m_p per patch:

$$m = m_b + 2m_p = \rho_b w_b t_b L_b \int_0^1 \varphi(\xi)^2 d\xi + 2\rho_p w_p t_p L_p \int_{\frac{x_1}{L_b}}^{\frac{x_1+L_p}{L_b}} \varphi(\xi)^2 d\xi \tag{31}$$

with $\xi = \frac{x}{L_b}$. Similarly for the modal stiffness:

$$k^E = k_b + 2k_p^E = \frac{Y_b I_b}{L_b^3} \int_0^1 \left(\frac{\partial \varphi(\xi)}{\partial \xi}\right)^2 d\xi + 2\frac{Y^E I_p}{L_b^3}(4 + 6\tau + 3\tau^2) \int_{\frac{x_1}{L_b}}^{\frac{x_1+L_p}{L_b}} \left(\frac{\partial \varphi(\xi)}{\partial \xi}\right)^2 d\xi \tag{32}$$

with $\tau = \frac{t_b}{t_p}$

The modal coupling is:

$$\theta_2 = \frac{d_{31} Y^E w_p t_p}{2L}(\tau + 1) \int_{\frac{x_1}{L_b}}^{\frac{x_1+L_p}{L_b}} \frac{\partial^2 \varphi(\xi)}{\partial \xi^2} d\xi \tag{33}$$

The same piezoelectric patch is chosen for the actuating PE, but is on the opposite side and with electrodes flipped, so $\theta_1 = \theta_2$. Finally the piezoelectric capacitance:

$$C_{p,2} = \frac{\varepsilon^S L_p w_p}{t_p} \tag{34}$$

For the parameters on Table 1, the modal mass is $m = 1$ kg, the closed and open circuit resonance frequencies are $\omega_{SC} = 430.85$ rad/s and $\omega_{OC} = 434.78$ rad/s , the modal electromechanical coupling coefficient $\theta_1 = \theta_2 = -0.0185$ C/m, the piezoelectric capacitance $C_p = 101$ nF and effective coupling of $k_{eff} = 0.14$.The modal damping of the beam was identified in Deweert (2019) as $c = 7.32$ Ns/m. The optimal resonant shunt according to equation (22) consists of $L_{opt} = 52$ H and $R_{opt} = 3766$ Ω. The frequency responses for the open circuit, closed circuit, ideal RL shunt and gyrator are depicted on Figure 8. These are computed from the expressions in section 3.1. The gyrator is tuned to 52 H as described in section 3.2. The closed-circuit resonance frequency $\omega_{SC} = 430.85$ rad/s is well below the tuning boundary of 1610 rad/s. The gyrator has a resistance of $R_{gyr}(\omega_{SC}) = 1180$ Ω so a resistor of $R_{add} = 2586$ Ω is added.

The well know superior performance of the resonant shunt is clearly seen on the FRF, with the typical equal-peaks characteristic of the tuning in equation (22). The gyrator closely mimics the ideal RL shunt, except for a small distortion near the peaks, where one peak higher than the other. For the resonant shunt and gyrator, the voltage over the circuit near resonance, see Figure 8b, is nearly the same as the applied voltage over the actuating piezo. In the experiment, the actuating voltage will be applied by an amplifier, which outputs a 200Vpp amplitude signal. To cope with this voltage level, the high-voltage design proposed above is required.

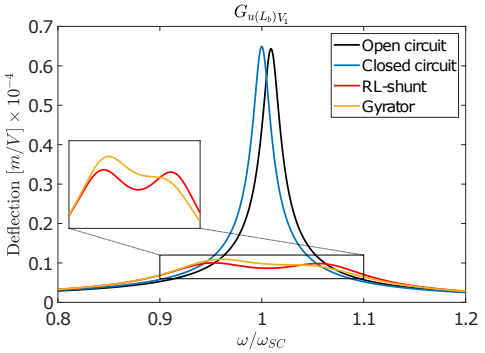

(a)

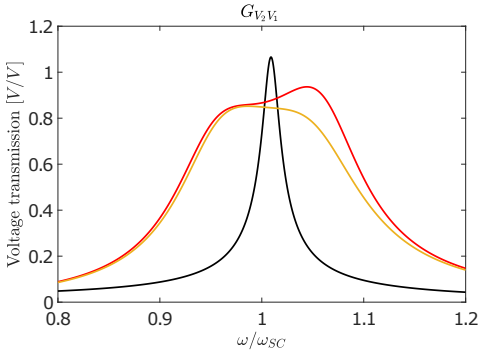

(b)

Figure 8. Simulated Frequency response function with V_1 as input and deflection at the tip $u(L_b)$ as output (a) and and shunt voltage V_2 as output (b) for PE2 open, resitive shunt and resonant shunt.

Beam		
L_b	Length	166 mm
w_b	Width	35 mm
t_b	Thickness	0.2 mm
Y_b	Young's Mod.	72 GPa
ρ_b	Mass Dens.	2800 kg/m^3
PE Mech.		
L_p	Length	50 mm
w_p	Width	30 mm
t_p	Thickness	0.02 mm
x_1	Offset	1 mm
Y^E	Young's Mod	62.2 GPa
ρ_p	Mass Density	7800 kg/m^3
PE Elec.		
ε^S	Dielectric const.	1750 nF/m
d_{31}	PE charge const.	-180 pC/N

Table 1. Constant of experimental setup, also used in simulations

3.4 Experiment

The cantilever beam setup in Figure 6 is experimentally built, see Figure 9c. The visible PEM patch is the actuating patch, while the PEM patch on the other side is connected to the gyrator, depicted in Figures 9a and 9b. The optimal resistance and inductance as tuned by equation (22) depend on closed and open circuit resonances. To identify these, a sine sweep with amplitude 100 V was applied to the actuating PE-patch with the other patch first in closed circuit, then open circuit. The deflection of the beam at the free end is measured with a laser vibrometer, the Keyence LK-G3000, and both the applied voltage and measured

deflection are used to construct an experimental frequency response function as shown on Figure 10a. The experimental open-circuit resonance frequency is 425.24 rad/s and the closed 421.72 rad/s. The generalized coupling coefficient, determined from the closed and open circuit resonance, is $k_{eff} = 0.13$, close to the theoretical coupling. The optimal shunt has $R_{opt} = 3706\ \Omega$ and $L_{opt} = 54$ H. The variable resistor on the gyrator, the rotary knob on the sides of the box in Figure 9a is set to synthetise L_{opt}. The internal resistance is $R_{gyr}(\omega_{SC}) = 1160\ \Omega$ and additional resistance is connected in series to obtain the optimal resistance. The experimental FRF with gyrator in Figure 10a, shows a significant, almost 10-fold decrease of the vibrations near the resonance of the cantilever beam.

To verify the high voltage over the RL shunt around resonance, the open circuit resonance frequency is applied to PE1 as a 200Vpp sine wave, while the voltage over PE is measured, once in open circuit and once when the RL shunt is applied, Figure 10b. The synthetic inductor can easily handle the measured voltage over the shunt (178Vpp), which would not be possible with conventional OpAmps, or with a single high-voltage OpAmp. Note that the applied voltage, 100V, corresponds to only 7 mm amplitude at the tip of the beam, Figure 10a when PE2 is in open or closed circuit.

The experimental FRF with gyrator is compared to the theoretical performance of an ideal RL shunt and a gyrator. All three have similar features and performance. Similar to to the theoretical gyrator performance, the experimental gyrator does not have the equal-peaks as the RL shunt has. Other deviations are attributed to inaccuracies in the identified damping, additional resistance and to the sensitive rotary kob of the experimental gyrator circuit, which is difficult to adjust precisely.

4 Conclusions

This research presented a high-voltage synthetic inductor consisting of 6 operational amplifiers, with an increased range from 100Vpp up to 400Vpp. At the heart of this circuit is a 1-OpAmp synthetic inductor, the gyrator. This way, resonants shunts are able to deal with the increasingly high vibration levels which induce high voltages in these shunts. By supplying a single gyrator circuit by output voltage boost configuration, where the supply of operational amplifiers depend on their output, the voltage range of the gyrator was doubled. Another doubling was achieved by then supplying two of these gyrators in an anti-phase manner. The frequency range where the gyrator can be tuned as an ideal resonant shunt were dreived. The circuit was designed and used as a shunt for a piezoelectric patch bonded to a cantilever beam. The experimental setup behaved similarly as its numerical model, with a 10 fold decrease of vibration level near resonance. The vibration in the beam induced voltages up to 178Vpp in the shunt, a voltage level where previous implementations of synthetic inductors are not able to deal with.

Conflict of interest

The authors declare no conflict of interest in preparing this article

Nomenclature

Symbol	Name
c	modal damping of mechanical system
C_L	Capacitor in gyrator
C_p	Piezoelectric capacitor
d_{31}	Piezoelectric charge constant
k^E	Closed circuit stiffness
k^D	Open circuit stiffness
k_{eff}	Effective modal coupling
L	Inductance
L_b	Beam length
L_p	Piezo length
L_{opt}	Optimal inductance in resontant shunt
m	modal mass of mechanical system
q	Charge in shunt
r	Modal displacement
R_{add}	Additional series resistance
R_{opt}	Optimal resistance in resonant shunt
R_{gyr}	Frequency dependent resistance of gyrator
R_L	Inherent resistor of gyrator
R_v	Variable resistor in gyrator for tuning inductance
t_b	Beam thickness
t_p	Piezo thickness
u	Beam deflection
V_1	Actuating voltage over actuating piezo
V_2	Voltage over shunt of damping piezo
Vpp	Peak-to-peak voltage
w_b	Beam width
w_p	Piezo width
Y_b	Young's modulus of beam
Y^E	Closed circuit Young's modulus of piezo
ε^S	Dielectric constant of piezo
θ	Modal electromechanical coupling coefficient
ρ_b	Mass density of beam
ρ_p	Mass density of piezo
φ	Mode shape of mechanical system
ω	Frequency
ω_{SC}	Closed circuit resonance frequency
ω_{OC}	Open circuit resonance frequency

References

APEX Microtechnology (2012) *P-876 DuraAct Patch Transducer*. URL https://www.apexanalog.com/resources/products/pa78u.pdf.

Berardengo M, Manzoni S, Thomas O and Vanali M (2018) Piezoelectric resonant shunt enhancement by negative capacitances: Optimisation, performance and resonance cancellation. *Journal of Intelligent Material Systems and Structures* 29(12): 2581–2606.

Chopra I and Sirohi J (2013) *Smart structures theory*, volume 35. Cambridge University Press.

dell'Isola F, Maurini C and Porfiri M (2004) Passive damping of beam vibrations through distributed electric networks and piezoelectric transducers: prototype design and experimental validation. *Smart Materials and Structures* 13(2): 299.

Den Hartog JP (1934) *Mechanical vibrations*. Courier Corporation.

Deweert R (2019) *Multimodal vibration damping with piezoelectric shunts*. Master's Thesis, Ghent University, Technology park 125.

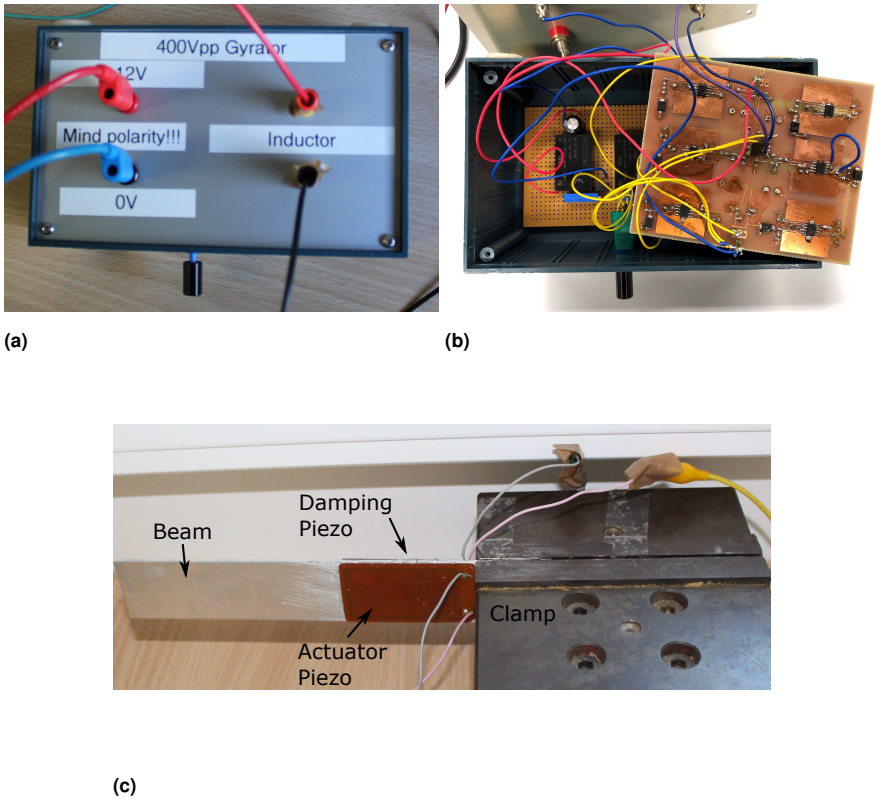

(a) (b)

(c)

Figure 9. The case of the 400Vpp synthetic inductor, closed (a) and open (b). The variable resistor is seen at the bottom center. The beam with PE patch bonded (c) on both sides.

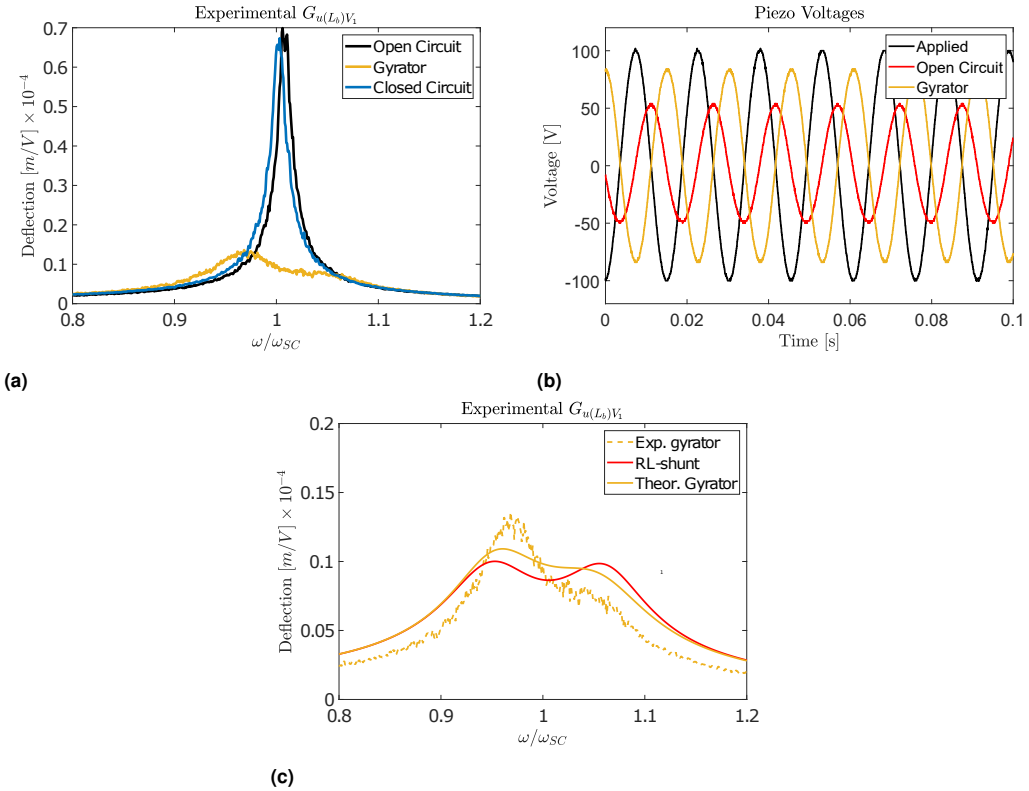

(a) (b)

(c)

Figure 10. Frequency response function with PE2 open, closed circuit and shunted (a) and resonant voltage applied to PE1 and generated by PE2 (b). The experimental response with gyrator compared to ideal RL shunt and theoretical gyrator (c) .

Hagood NW and von Flotow A (1991) Damping of structural vibrations with piezoelectric materials and passive electrical networks. *Journal of Sound and Vibration* 146(2): 243–268.

Heuss O, Salloum R, Mayer D and Melz T (2016) Tuning of a vibration absorber with shunted piezoelectric transducers. *Archive of Applied Mechanics* 86(10): 1715–1732.

Leo DJ (2007) *Engineering analysis of smart material systems*. Wiley Online Library.

Lossouarn B, Aucejo M, Deü JF and Multon B (2017) Design of inductors with high inductance values for resonant piezoelectric damping. *Sensors and Actuators A: Physical* 259: 68–76.

National Semiconductor (1994) *Linear Applications Handbook*.

Nečásek J, Vaclavik J and Marton P (2016) Digital synthetic impedance for application in vibration damping. *Review of Scientific Instruments* 87(2): 024704.

Neubauer M, Oleskiewicz R, Popp K and Krzyzynski T (2006) Optimization of damping and absorbing performance of shunted piezo elements utilizing negative capacitance. *Journal of sound and vibration* 298(1-2): 84–107.

PI ceramics (2008) *Piezoceramic Materials*.

PI ceramics (2020) *DuraAct Patch Transducer*. URL https://static.piceramic.com/fileadmin/user_upload/physik_instrumente/files/datasheets/P-876-Datasheet.pdf.

Texas Instruments (2008) *High Voltage FET-Input OPERATIONAL AMPLIFIER*.

Texas Instruments (2016) *OPA454 High-Voltage(100 V),High-Current(50 mA) Operational Amplifiers , G=1 Stable*. URL https://www.ti.com/lit/ds/symlink/opa454.pdf.

Thomas O, Ducarne J and Deü JF (2011) Performance of piezoelectric shunts for vibration reduction. *Smart Materials and Structures* 21(1): 015008.

Vatavu M, Nastasescu V, Turcu F and Burda I (2019) Voltage-controlled synthetic inductors for resonant piezoelectric shunt damping: A comparative analysis. *Applied Sciences* 9(22). DOI:10.3390/app9224777. URL https://www.mdpi.com/2076-3417/9/22/4777.

Wang G, Cheng J, Chen J and He Y (2017) Multi-resonant piezoelectric shunting induced by digital controllers for subwavelength elastic wave attenuation in smart metamaterial. *Smart Materials and Structures* 26(2): 025031.